

Towards Scalable Multi-Chip Wireless Networks with Near-Field Time Reversal

Ama Bandara*, Fátima Rodríguez-Galán*, Pau Talarn, Elana Pereira de Santana, Peter Haring Bolívar, Eduard Alarcón, Sergi Abadal

Abstract—The concept of Wireless Network-on-Chip (WNoC) has emerged as a potential solution to address the escalating communication demands of modern computing systems due to their low-latency, versatility, and reconfigurability. However, for WNoC to fulfill its potential, it is essential to establish multiple high-speed wireless links across chips. Unfortunately, the compact and enclosed nature of computing packages introduces significant challenges in the form of Co-Channel Interference (CCI) and Inter-Symbol Interference (ISI), which not only hinder the deployment of multiple spatial channels but also severely restrict the symbol rate of each individual channel. In this paper, we posit that Time Reversal (TR) could be effective in addressing both impairments in this static scenario thanks to its spatiotemporal focusing capabilities even in the near field. Through comprehensive full-wave simulations and bit error rate analysis in multiple scenarios and at multiple frequency bands, we provide evidence that TR can increase the symbol rate by an order of magnitude, enabling the deployment of multiple concurrent links and achieving aggregate speeds exceeding 100 Gb/s. Finally, we evaluate the impact of reducing the sampling rate of the TR filter on the achievable speeds, paving the way to practical TR-based wireless communications at the chip scale.

Index Terms—Time Reversal; Near-Field Communications; Wireless Interconnects; Network-on-Chip

I. INTRODUCTION

The end of Moore’s law has compelled computer architects to explore methods for improving the performance and efficiency of microprocessors beyond mere transistor scaling. One approach involves increasing the number of independent processor cores within a chip, resulting in what are known as many-core processors [1]. Alternatively, other strategies encompass the deployment of specialized hardware accelerators and the integration of multiple such specialized chips within a computing package [2]. Given the parallel nature of these architectures and their requirement for internal data synchronization and sharing, effective communication within and between chips emerges as a pivotal factor determining the performance and efficiency of next-generation computing systems.

Currently, numerous processor families in both academic and industrial settings adopt the Network-on-Chip (NoC) as

the prevailing solution for on-chip communications [1]. A NoC functions as a packet-switched network comprising on-chip routers and links co-integrated into the architecture. Its widespread use is attributed to its simplicity and high performance, particularly in moderately sized processors. However, as architectures scale towards larger sizes and extend beyond the confines of a single chip, where wired links experience significant slowdowns [2], NoC encounters notable challenges related to latency and energy consumption. This becomes especially problematic during collective communications, such as one-to-all and all-to-one patterns, which can lead to severe congestion within the NoC.

In this context, Wireless Network-on-Chip (WNoC) is an emerging paradigm with significant promise to enhance communications within computing packages. WNoC are possible because of the advances in antennas and transceivers in the millimeter-wave (mmWave) and THz bands that have made possible their integration inside computing cores [3], [4]. They are expected to solve the scalability and flexibility issues that come with the increment of the number of processors, their integration on multiple interconnected chips, and the use of wired NoC communication approaches [1], [5]. The goal is to augment the wired backbone with wireless links within the package [6].

Due to the use of electromagnetic (EM) propagation nearly at the speed of light, WNoC provides broadcast and multicast opportunities with reduced latency and is expected to offer reconfigurable links able to operate at speeds of tens of Gb/s or more. For the WNoC paradigm to be competitive, though, it must deliver a reliability commensurate to that of their wired counterpart. In particular, multiple works [7]–[10] point towards a latency of 1–10 nanoseconds, a throughput in the range of 10–100 Gb/s or higher, and a Bit Error Rate (BER) of 10^{-12} – 10^{-15} as targets for WNoC. Complying with these values while keeping low the area/power consumption calls for affordable solutions, low order modulations, and simple physical layer elements for implementation [9], [11]–[15].

However, several challenges arise when including wireless communications in a package environment while trying to meet the target performance requirements. Some examples include the antenna placement in the highly integrated environment, design of transceivers with efficient coding schemes and modulations, interference management, and medium access control [6], [16]–[18]. In particular, in this paper we focus on the problems of inter-symbol interference (ISI) and co-channel interference (CCI). In the on-chip scenario, the antennas radiate in a highly reverberant environment and are

*F. Rodríguez-Galán and A. Bandara contributed equally to this work. Authors acknowledge support from the European Union’s Horizon 2020 research and innovation program, grant agreement 863337 (WiPLASH), the European Research Council (ERC) under grant agreement 101042080 (WINC) as well as the European Innovation Council (EIC) PATHFINDER scheme, grant agreement No 101099697 (QUADRATURE). Corresponding author: Sergi Abadal (abadal@ac.upc.edu)

A. Bandara, F. Rodríguez-Galán, P. Talarn, E. Alarcón, S. Abadal are with Universitat Politècnica de Catalunya, Spain. E. Pereira de Santana and P. Haring Bolívar are with University of Siegen, Germany

impaired by near-field effects. As a result, on the one hand, signals are subject to multiple reflections before reaching the receiver, leading to large delay spreads dominated by the strong multipath components. This leads to severe ISI, which degrades the performance of high-rate transmissions especially in low-order modulations. On the other hand, reverberation causes the radiated energy to spread across the entire space. This leads to strong CCI with non-intended antennas and prevents the possibility of having multiple spatial channels concurrently.

Time Reversal (TR) [19]–[23] is a technique that uses a time-reversed version of the channel’s impulse response (CIR) to create a matched filter that focuses energy in space and time in a targeted destination. Due to the spatiotemporal focusing, TR can therefore considerably alleviate both ISI and CCI, as shown in multiple works at multiple scales and including in the near-field [20], [24].

In traditional large-scale wireless systems, this approach is expensive to implement because the channel, being dynamic, would have to be estimated continuously. In the chip scenario, however, the node position is fixed and every element in the system is known. This works to our advantage because regardless of the channel complexity, this will be almost fixed and static. One estimation of the CIR of the wireless path between terminals of interest will remain constant and can be used in every transmission. Moreover, the near-field effects naturally arising in WNoC due to the small scale of the chip environment are not an issue, since TR can be applied to channels with near-field effects as long as their consequences are captured in the CIR [20], [24].

In previous work, we explored TR in a small set of chip configurations and frequencies [25], [26]. In [25], we proposed TR in a flip-chip structure at 60GHz to mitigate the ISI of single-link communications. Moving forward, in [26] we aimed for a TR approach for multiple simultaneous channels at 140GHz, in a multi-core architecture to mitigate CCI (Figure 1). We were able to show the superiority BER-wise of using TR to successfully transmit at high data rates and get rid of undesired interference. However, in this past work, besides assuming a limited set of environments, we considered an ideal TR filter that can compensate perfectly for all the components of the channel. Perfect filters are impossible to fabricate in practice, and in this scenario, a high-resolution filter might be unfeasible due to area/power constraints.

In this work, we expand beyond our prior work with a deep exploration of the effectiveness of TR in a broader set of settings and using filters with a finite sampling rate. In particular, the contributions of this paper are as follows:

- We formulate, simulate, and evaluate the performance of wireless links in a four-chiplet computing system at 140 GHz (Figure 1), in single-link and multi-link settings, with and without time reversal. We observe order of magnitude improvements on the speed of the links, and the possibility to deploy multiple links concurrently.
- We assess the impact of changing the frequency of operation of the wireless link without modifying the environment. We observe that time reversal is compatible

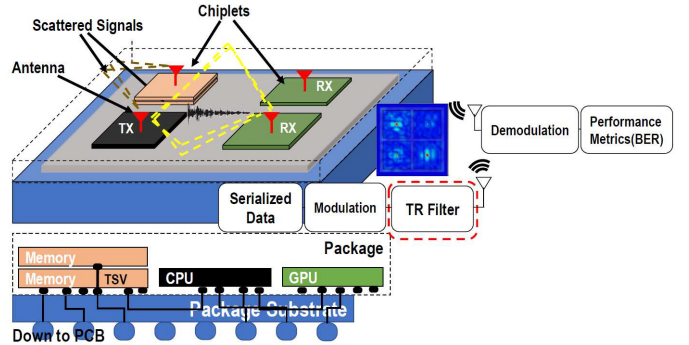


Fig. 1: Overview of the application of time reversal in a wireless network within package. Modulated data is transmitted through the proposed TR filter and focused on the intended receivers.

with all frequencies in this environment, without large variations in performance.

- We assess the impact of changing the environment, by modifying the number of chiplets and their size. We observe that these changes can have an impact on the performance of the wireless links.
- We consider filters with a finite sampling rate and evaluate the degradation of performance as the sampling rate is reduced. We observe gradual reductions in the achievable speeds due to an increasing mismatch between the CIR and the TR filter.

The rest of the paper is organized as follows. In Section II, we provide some background related to the general problems of the on-chip scenario. In Section III, we formulate the system model considered throughout this work. In Section IV, we describe the overall evaluation methodology, including the simulation pipeline, the simulated environment, and the evaluated variations. In Section V, we present the results obtained from the base scenario, which is used as base for the parametric characterization developed in this work. In Section VI, we evaluate the performance of TR for changes in the operation frequency and the geometry of the chip. Finally, in Section VII, we use a sample-and-hold filter with variable sampling rate to assess the trade-off between performance and feasibility of TR in this scenario.

II. BACKGROUND

A. Wireless Communications at the Chip Scale

Wireless communications on chip-scale have been built with the foundation of using millimeter wave technology for electromagnetic nano-communication, as an overlay of wireless links on top of wired NoC architecture. A variety of antennas and transceivers [27]–[32] have been proposed to be co-integrated as a system in package, where the wireless channel inside the chip is chosen as the propagation medium. WNoC complements NoC nicely with reconfigurability, low latency, and broadcasting capabilities for a high number of cores (> 64). In a dense wired routing network, WNoC can avoid unnecessary hops when communicating distant cores.

To meet the expected performance of WNoC with high data rates and ultra-low latency, the wireless channels have

to be shared among the antennas or the modulation order data transmissions have to be increased. Therefore MAC protocols play an important role in maintaining reliable data communication, where several attempts have been made [17], [33]–[35] to adapt token-passing, CSMA to the chip environment by considering its unique requirements and characteristics. On the other hand, although the modulations are also crucial on enhancing the data rate, the area, power overhead of the chip scale transceivers and stringent BER requirements have limited the modulations to On off keying (OOK) [36], [6].

B. Wireless Channel within the Chip Package

The controlled materials and dimensions within the chip package let us tailor the wireless channel and know the nature of the medium beforehand [13], [37], [38]. A computer chip is created by stacking layers of lossy silicon, metal, and dielectric [39]. In particular, the structure of the flip-chip configurations widely used in nowadays processors is, from top to bottom: a heat sink on top, the silicon substrate, a thin dielectric layer for the interconnections, and a layer of solder bumps that connect the chip to the PCB [40]. Recently, a trend in computer architecture consists in the interconnection of multiple flipped chips in a co-planar configuration. To this end, the chips are connected through a silicon interposer with a much higher connection pin density than via a PCB [41], [42]. All the work developed in this paper considers such a 2.5D integration scheme.

Regardless of the number of interconnected chips, communicating within the chip package with electromagnetic radiation has its unique characteristics. A large amount of the transmitted energy will be reflected by the metal enclosure, the edges, and obstacles in the structure, leading to a large delay spread with multi-path propagation while creating a distinctive CIR between each transmitter and receiver [13], [37]. Fortunately, the structure is designed beforehand, and all materials, nodes, and terminals will become fixed and known. This offers a significant advantage since the wireless channel can be treated as quasi-deterministic and time-invariant which enables a pre-characterization of the CIR that will not change and that requires a single estimation process and can be reused moving forward.

C. Time Reversal for On-Chip Communications

TR is a technique that can be used to compensate for the multipath effects that occur in complex transmission mediums with the use of adaptive energy focusing on the pre-characterized CIRs. The phase conjugate of the CIR is obtained, pre-emphasized with the transmitting symbols, and propagated through the same wireless medium such that the radiated energy is focused in both time and space at a target receiver. TR acts as an ideal spatial matched filter with the process of auto-correlation of the transmitted time-reversed channel response with an equal wireless medium.

As the chip-scale wireless communications are conducted in quasi-deterministic channels, TR is a promising technology to adapt as a solution to mitigate the ISI effects that occur due

to energy reverberation. With prior known wireless channels, repetitive CIR characterization is not required.

Channel correlation plays a crucial role in TR processing and the energy focusing could be for the merit or adverse based on the expected signal transmission scenario. Even though TR was initially adapted for on-chip communications to mitigate ISI, later it was proved that TR could be used to reduce the co-channel interference in same frequency/time signal transmissions [25], [26]. When the communicating channels are less correlated TR is capable of reducing the non-orthogonal interference of nearby signal transmissions with the use of destructive cancellation of energy components on focused CIR. In return, it enables the wireless medium to have parallel concurrent signal transmissions by sharing the same bandwidth, thus improving the aggregate data rate of the system. However, this phenomenon is adverse with symmetric channels where the co-channel interference could be high. In such cases, the known CIR can be analyzed before the transmissions to optimize the communication scheme. Nevertheless, the symmetric channels can be highly useful to focus the energy on multiple nodes with single transmitter excitation to enhance the broadcasting capabilities.

III. SYSTEM MODEL

In this section, we provide a detailed description of the TR process and its influence on the transmission. The model is detailed for different scenarios involving one or more concurrent TR links.

A. TR with Single Input Single Output Link

We analyze the case of TR-based adaptive energy focusing on time domain. Let us consider, for the purpose of characterisation, that an impulse is excited from an arbitrary transmitter i to an arbitrary receiver k . The characterized CIR is recorded and used to transmit modulated information via the channel h_{ik} , which is given by

$$h_{ik}(t) = \sum_{n=1}^N A_n e^{j\theta_n} \delta(t - \tau_n), \quad (1)$$

where $\{A_n, \theta_n, \tau_n\}$ are amplitude, phase, and propagation delay of the multipath component n of the CIR h_{ik} .

For simplicity, impulse radio OOK modulated symbols are assumed. Hence, symbols $m_{ik} \in \{1, 0\}$, are sent through the characterized time-reversed filter and transported towards receiver k from the transmitter i . The transmitted signal can be expressed as

$$s_{ik}(t) = h_{ik}^*(-t) \star m_{ik} \quad (2)$$

where $(\cdot)^*$ represents the complex conjugate operator and \star indicates the convolution operator respectively.

The resultant energy concentration resembles the autocorrelation of the CIR as

$$\begin{aligned} y_{ik}(t) &= \{s_{ik}(t)\} \star h_{ik} + n_k \\ &= m_{ik} \star h_{ik}^*(-t) \star h_{ik} + n_k \\ &= m_{ik} \star R_{ik}^A(t) + n_k \end{aligned} \quad (3)$$

where $R_{ik}^A(t)$ denotes the autocorrelation function of the channel h_{ik} and n_k is the Additive White Gaussian Noise (AWGN) component at the receiver k . The autocorrelation property eliminates the multipath effects with constructive and destructive interference cancellation while improving the signal-to-noise ratio (SNR) at the respective receiver.

Next, we assume a case where the transmitted signal s_{ik} is propagated towards an off-target receiver k' . Then,

$$\begin{aligned} y_{ik'}(t) &= \{s_{ik}(t)\} \star h_{ik'} + n_{j'} \\ &= m_{ik} \star R_{ikk'}^C(t) + n_{j'} \end{aligned} \quad (4)$$

where $R_{ijj'}^C(t)$ represents the cross correlation function in between the arbitrary channels h_{ij} and $h_{ij'}$. For further analysis of the impact of channel correlation functions on TR, let us consider the convolution of the CIR $h_{ik'}$ with the time-reversed h_{ik}^* :

$$h_{ik'}(t) \star h_{ik}^*(-t) = \int_{-\infty}^{\infty} h_{ik'}(\tau) h_{ik}^*(-(t-\tau)) d\tau \quad (5)$$

By substituting Equation (1) in Equation (5), the convolution operation can be obtained as

$$\begin{aligned} h_{ik'}(t) \star h_{ik}^*(-t) &= \int_{-\infty}^{\infty} \sum_{n'=1}^{N'} A_{n'} e^{j\theta_{n'}} \delta(\tau - \tau_{n'}) \\ &\quad \sum_{n=1}^N A_n e^{-j\theta_n} \delta(-(t-\tau) - \tau_n) d\tau \end{aligned} \quad (6)$$

where $\{A_{n'}, \theta_{n'}, \tau_{n'}\}$ are amplitude, phase, and propagation delay of the multipath component n' of the CIR $h_{ik'}$.

Thus the simplified cross-correlation expression can be obtained as

$$R_{ikk'}^C(t) = \sum_{n'=1}^{N'} \sum_{n=1}^N A_{n'} A_n e^{j(\theta_{n'} - \theta_n)} \delta(t - (\tau_{n'} + \tau_n)) \quad (7)$$

With the above expression, it is observed that when the transport signal is passed through symmetric channels (autocorrelation index is high) the energy components are constructively added with a null phase shift while having the maximum energy concentration at the point of maximum propagation delay; $\max(\tau_n)$. When the TR adopted CIR is dissimilar, the cross-correlation index is phase shifted and the energy concentration will be controlled by the shifted amount of phase. As the EM waves are propagated through an enclosed chamber, it is complex to predict the randomness of the CIR. Thus, it is important to measure each CIR before the transmissions and design the protocols to optimize the paths in parallel communications.

B. TR with Multiple Input Multiple Output Link

Subsequently, let us consider multiple input multiple output (MIMO) communication with TR. In the cases that follow, suppose there are N_t transmitters with N_r receivers simultaneously communicating with each other on an interposer package.

1) *Single Transmitter-Multiple Receivers*: First, let us consider a scatter operation from a single transmitter to multiple receivers. In computer architecture, scatter refers to the distribution of $P = \{p_1, \dots, p_N\}$ pieces of data to N receivers with a one to one mapping, i.e. p_1 to node 1, p_2 to node 2, etc. Assuming that all the wireless channels are pre-characterized, the TR modulated symbols to be transmitted from i^{th} single transmitter to the k^{th} receiver can be expressed as

$$s_{ik}^t(t) = \sum_{k'=1, k' \neq k}^{N_r} h_{ik'}^*(-t) \star m_{ik'} + h_{ik}^*(-t) \star m_{ik} \quad (8)$$

TR precoding is done based on the simultaneous transmissions utilized in the particular transmitter to the intended receivers. Note that according to the receiver selection, other TR-CIR can be assumed as zero.

The received signal from a single i^{th} transmitter to k^{th} receiver can be obtained as

$$\begin{aligned} y_{ik}^t(t) &= s_{ik}^t(t) \star h_{ik} + n_k \\ &= \left\{ \sum_{k'=1, k' \neq k}^{N_r} h_{ik'}^*(-t) \star m_{ik'} + h_{ik}^*(-t) \star m_{ik} \right\} \star h_{ik} \\ &\quad + n_k \\ &= \underbrace{\sum_{k'=1, k' \neq k}^{N_r} R_{ikk'}^C(t) \star m_{ik'}}_{\text{Interference}} + \underbrace{R_{ikk}^A(t) \star m_{ik}}_{\text{Signal}} + n_k \end{aligned} \quad (9)$$

Based on the measurements of the channel correlation index among the characterized CIR, the interference can be previously known. Although the effects of interference could be decreased as discussed in Equation (6), it is important to measure the amount of decrement to learn the number of simultaneous transmissions that can be utilized.

2) *Multiple Transmitters-Multiple Receivers*: Second, let us consider a scenario when multiple transmitters transmit to multiple receivers. This scenario resembles a parallel information shared in between cores, to improve the aggregate data rate of the system. Here, each i^{th} transmitter wishes to transmit the TR precoded modulated information to the intended receiver k . Thus, the transmitted signal can be obtained as

$$s_{ik}^r(t) = \sum_{i'=1, i' \neq i}^{N_t} h_{i'k}^*(-t) \star m_{i'k} + h_{ik}^*(-t) \star m_{ik} \quad (10)$$

The received signal at a single k^{th} receiver can be expressed as

$$\begin{aligned} y_{ik}^r(t) &= s_{ik}^r(t) \star h_{ik} + n_k \\ &= \left\{ \sum_{i'=1, i' \neq i}^{N_t} h_{i'k}^*(-t) \star m_{i'k} + h_{ik}^*(-t) \star m_{ik} \right\} \star h_{ik} \\ &\quad + n_k \\ &= \underbrace{\sum_{k'=1, k' \neq k}^{N_r} R_{i'kk}^C(t) \star m_{i'k}}_{\text{Interference}} + \underbrace{R_{ikk}^A(t) \star m_{ik}}_{\text{Signal}} + n_k \end{aligned} \quad (11)$$

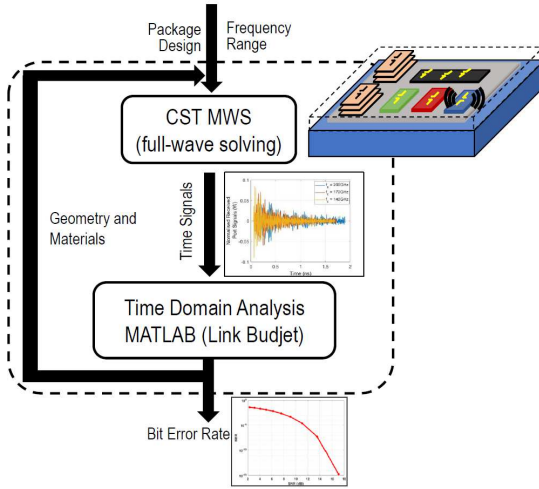


Fig. 2: Summary of the proposed methodology: Characterisation of channel impulse response and analyzing the proposed communication with MATLAB

As we observe in Equation (11), the interference is dependent on the channel cross-relation between the focused channel CIR with the interference channels (refer to Fig. 3) due to the non-orthogonality of the signal transmissions. It is advisable to measure the correlation of each channel prior to the signal transmissions and manage the communications with an adaptable MAC protocol.

C. SINR Analysis with TR

To quantify the impact of TR on the effectiveness of the signal transmission, the signal-to-noise plus interference ratio was measured for both single-link and multi-link TR precoded communications. Even though ISI is highly mitigated with TR, it is important to quantify the peak energy concentration proportional to the data rate to measure how much concentration we could achieve with closely packed energy peaks in higher data rates.

We detect the peak energy concentration inside a defined time domain window with general energy detection [43] based on the data rate and consider the energy outside the defined time duration as the interference due to low-compressed energy components. The SINR is defined for three cases as aforementioned in Section III-A and Section III-B. Therefore, SINR for single input single output channel can be obtained as,

$$SINR_{SISO} = \frac{\int_{t_1}^{t_2} y_{siso}(t)^2 dt}{I_{siso} + n_k} \quad (12)$$

where, $y_{siso}(t) = m_{ik} \star R_{ik}^A(t)$, $I_{siso} = \int_0^{t_1} y_{siso}(t)^2 dt + \int_{t_1}^{2max(\tau_n)} y_{siso}(t)^2 dt$, $t_1 = max(\tau_n) - t_{rate}/2$, $t_2 = max(\tau_n) + t_{rate}/2$. t_{rate} is the defined time domain window for the energy detection.

Similarly, based on the received signals as in Equation (9) the SINR for single transmitter multiple receivers can be obtained as

$$SINR_{SIMO} = \frac{\int_{t_1}^{t_2} y_{simo}(t)^2 dt}{I_{siso} + I_{CCI}^t + n_k} \quad (13)$$

TABLE I: Evaluated Structure and Dimensions.

Parameter	Thickness	Materials	Units
Lateral Spacer	-	Vacuum	N/A
Heat Spreader	0.5	Aluminum Nitride	mm
Silicon die	0.5	High-res. Silicon	mm
Chiplet insulator	0.01	SiO ₂	mm
Bumps	0.0875	Copper	mm

TABLE II: Evaluation Scenarios.

Variables	Default	Section	Variations	Section
No. chiplets	4		4–16	Sec. VI
Frequency (GHz)	140	Sec. V	140–170	Sec. VI
Sampling Rate (GHz)	Ideal		80–400	Sec. VII

where $y_{simo}(t) = m_{ik} \star R_{ik}^A(t)$, $I_{simo} = \int_0^{t_1} y_{simo}(t)^2 dt + \int_{t_1}^{max(\tau_n + \tau_{n'})} y_{simo}(t)^2 dt$, $I_{CCI}^t = \int_{t_1}^{t_2} \{R_{i'kk'}^C(t) \star m_{i'k'}\}^2 dt$.

Subsequently, with the received signal in equation (11) the SINR for multiple transmitters and multiple receivers can be expressed as below.

$$SINR_{MIMO} = \frac{\int_{t_1}^{t_2} y_{mimo}(t)^2 dt}{I_{mimo} + I_{CCI}^r + n_k} \quad (14)$$

Where, $y_{mimo}(t) = m_{ik} \star R_{ik}^A(t)$, $I_{mimo} = \int_0^{t_1} y_{mimo}(t)^2 dt + \int_{t_1}^{max(\tau_n + \tau_{n'})} y_{mimo}(t)^2 dt$, $I_{CCI}^r = \int_{t_1}^{t_2} \{R_{i'kk'}^C(t) \star m_{i'k'}\}^2 dt$.

IV. METHODOLOGY

The overview of the proposed methodology is shown in Fig. 2. We follow a sequential methodology for this work to (1) systematically pre-characterize the wireless channel with CIR by using CST Microwave Studio [44] and (2) model the communication system on MATLAB to analyze the performance of the TR technique on modulated streams of data. We detail them next.

A. Full-wave Simulation

The simulations made in this work are conducted in an interposer. The detailed configuration of the flip-chip layers is seen in Table I. To create the interposer we placed a number of flip-chip structures on top of a stack of silicon interposer and two layers of copper. The space between chiplets is filled with vacuum and the configuration is completely enclosed by a Perfect Electric Conductor (PEC). Each chiplet is augmented with a number of antennas placed in symmetrical positions in a Trough-Silicon-Vias (TSV) approach [25] as vertical monopoles. Unless noted, we consider four chiplets with three antennas per chiplet tuned at a frequency of 140 GHz.

Moving forward we developed several simulations to study the TR technique, its behavior, and application possibilities for changes in the base scenario in terms of frequency of operation and changes in the structure's geometry. We refer the reader to Table II for details on the evaluated variations.

The structures where the parametric sweep takes place are seen in Figure 3. We illustrate the location of the antennas and the links used for measurement of the quality of transmission. As observed, we change the number of chiplets to study the impact of the layout on the effectiveness of TR. In particular,

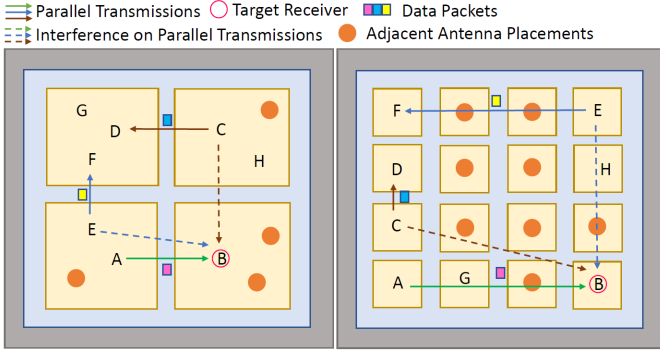


Fig. 3: Evaluated multi-receiver time-reversal scenarios for four and sixteen chiplets in an interposer package, with multiple concurrent transmitters at the same time, different data to different receivers.

we introduce more chips in the same amount of space, hence decreasing the chiplet size and only placing one antenna per chiplet.

Each scenario is simulated in CST Microwave Studio using the time-domain solver. The length of the vertical monopole antennas is adjusted to resonate in frequencies close to 140, 170, and 200 GHz (Fig. 4a). We can also see several notches, which suggest that we are indeed in a reverberant scenario with significant near-field effects; the antenna can couple with nearby and distant elements, changing the impedance and hence mismatching the antenna. As a result, we also need to adapt the antenna when varying the dimensions of the chiplet (Fig. 4b).

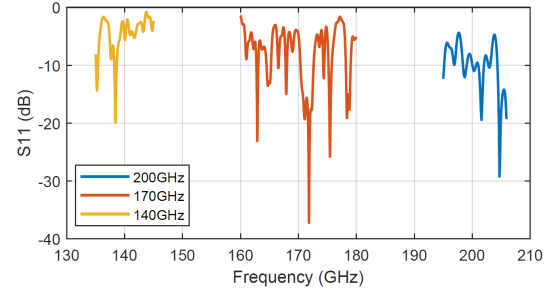
Once the antennas are modeled correctly, we apply an impulse to the transmitting antenna to obtain the CIR at the output. Hence, the outcome of the simulations is the CIR from a given port to all others. Hence, we obtain information to evaluate any wireless link we consider for transmission. This can be extracted from the software and further processed in MATLAB.

Finally, we note that, to validate the time reversal approach, we record the CIR and excite the transmitting antenna with the reversed version of the CIR. This simulation is used to obtain the field distribution and see the spatiotemporal focusing, as well as to later compare the results with that of a simple convolution between the filter and the actual channel in MATLAB.

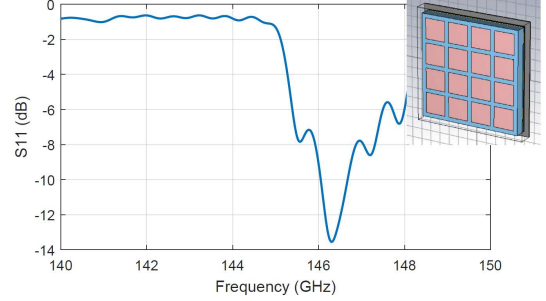
B. PHY Layer Simulation

As the next step, the characterized CIR is used to process the proposed communication scheme with TR. First, we generate a pseudo-random string of bits with the preferred data rate. The data is then modulated with impulse radio (IR) on-off keying (OOK) modulation to create a train of impulses, although the methodology is easily applicable to continuous-wave modulations, in which case the data would be multiplied by a continuous time carrier wave with a frequency matching the antenna resonance frequency.

In transmission, the modulated symbols are convoluted with the TR filters and transported in the wireless channel. AWGN noise is added to the transport signal and the noise power is



(a) Return loss for antennas at 140/170/200 GHz, four chiplets.



(b) Return loss for antenna at 140 GHz, sixteen chiplets.

Fig. 4: Return loss of the simulated antennas in the multiple evaluated scenarios.

modeled as $P_{AWGN} = KTB$, where K is the Boltzmann constant, T is the chip temperature and B is bandwidth. The TR filter is initially modeled as the ideal (continuous) time-reversed CIR perfectly matching the characterized channel. However, in Section VII, we also perform a gradual degradation of the filter sampling rate in the default simulated scenario to consider a more realistic filtering approach and observe the resulting degradation in performance of the wireless link.

At the receiver, Energy Detection (ED) is implemented by integrating the received signals (aforementioned in Section III) over the respective time intervals based on the data rate. The computed energy values are compared with a threshold to decode the data stream. The threshold value is decided a posteriori and on a per-link basis to minimize the BER.

V. TIME REVERSAL IN A MULTI-CHIP SCENARIO

For the baseline scenario, the simulations have been executed for several transmission cases in a four-chiplet scenario at 140 GHz and assuming ideal filters. Also, the links contemplated are within the same chip and among different chips. The results entail single-link and multiple-link transmissions. Within the multiple links scenario, we made simulations for multiple transmitters and multiple receivers.

Figure 5 shows a summary of the results of TR obtained with our end-to-end methodology. Fig. 5(a) illustrates the spatiotemporal focusing of the technique (right) in comparison with normal transmission (left). We can see the cleanness of the TR transmission with high concentration in targeted spots and low concentration elsewhere, except for symmetric points. On the other hand, the electrical field in the non-TR case is completely scattered, with some concentration in the desired

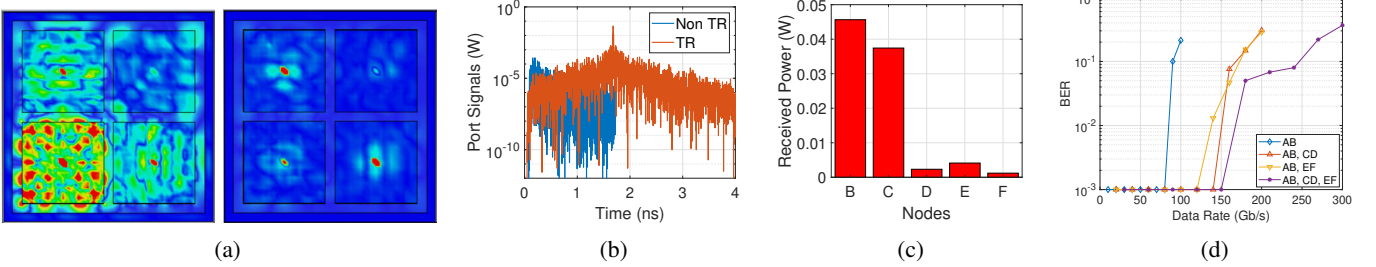


Fig. 5: Single-link time-reversal with vertical monopoles in an interposer package at 140 GHz. (a) Spatial distribution of field before and applying TR. (b) Signal received over time in node *B* before and after applying TR. (c) Total received power in the intended receiver *B* and non-intended receivers *C–F*, (d) BER as a function of the aggregated data rate for a total power of 10 dBm in the TR case. See [26] for more details.

target but surrounded by large amounts of interference, which tarnishes any concurrent transmission attempt.

As we further show in Fig. 5(b), the TR signal at the receiver is focused in the time domain, showing a large and very concentrated peak of 45 mW; whereas the non-TR signal appears spread and with the peak only reaching 0.2 mW.

With respect to co-channel interference, an important conclusion can be drawn from Fig. 5(c). This image shows the ability of TR to compress the energy concentration in non-desired targets if and when the channel impulse response of each wireless path is not correlated with the targeted receiver. In this particular case, node *C* is placed in a relatively symmetric position with respect to the targeted node *B* and, hence, receives a relatively large interference. An opposite behavior is observed for nodes *D* to *F*, for which the interference is largely suppressed.

To evaluate the performance of TR with parallel communications, the BER as a function of the aggregated data rate (i.e. the sum of the data rates of all parallel transmissions) is measured as illustrated in Fig. 5(d). It was observed that even with three concurrent communications, the SINR is higher than non-time reversal transmissions, and thus the BER is improved at the receiver. In terms of data rate, a significantly high aggregate data rate can be obtained with time reversal. In particular, a speed of 50 Gb/s is obtained with an error rate below 0.01 with a single-link transmission. Compared with the non-TR transmission (not shown here), the TR case achieves an order of magnitude higher speed for the same BER. Further, as we add new concurrent links to the simulation, we observe that the aggregate data rate increases with the number of deployed, although the system starts to saturate with three concurrent links in this particular case. In summary, these results are indicative of the capacities of TR.

VI. SENSITIVITY ANALYSIS

Next, we want to determine the limits of our model and explore possible shortcomings that arise from changes in the structure as well as variations with the frequency.

A. Impact of Communication Frequency

As it is beneficial to count with multiple frequencies for transmission, the TR evaluation is made also for multiple frequencies, maintaining the rest of the interposer landscape

intact. The peak energy concentration with TR on the focused receiver is based on two main factors such as the delay spread and the received signal strength of the characterized CIR. When the center frequency of the antenna is increased, the delay spread generally tends to get shorter, and based on the scattered energy components on the chip package, the received signal strength on each antenna could be increased or decreased. This variation in frequency affects the receiver's peak energy concentration and thus the system's bit error rate. We evaluate these effects next.

Fig. 6 shows the general behavior of characterized CIR and the received peak energy concentration with different antenna resonance frequencies. It is observed that, even with a short delay spread, a clean focused energy peak is obtained at all frequencies. The specific peak instantaneous power and the width of the response depends on the length of the CIR and total energy of the CIR. While we observe some variations on these values, there is not a specific trend or large impact. This is because the scenario keeps being fairly reverberant at all frequencies, and the TR filter is adapted to each new measured CIR.

To assess the degree of spatial focusing of our technique, we evaluate the ratio of the power in the desired target to the power of the rest of ports of the system. As observed in Figure 6c for a particular link, we observe how TR focuses the energy on the target destination, as the power is superior to the sum of the powers in all the other ports. In contrast, the non-TR case will probably lead to large co-channel interference, since the power at the intended destination is just a small fraction of the power arriving to all other ports. The difference between both cases is around $3\times$ with small variation when changing the operation frequency of the wireless network. Hence, this confirms that TR could be used simultaneously to frequency multiplexing in a single package.

The TR capabilities have been further tested by obtaining the BER as a function of the data rate of an OOK modulated stream in all frequencies. The results, summarized in Fig. 6d for a fixed BER of 0.1, show a consistent behavior of the TR technique. In general, it is observed that TR works well at all frequencies, with a large gap between the non-TR and TR achievable rates. As the frequency increases, the performance of TR can increase or decrease depending on the particular shape of the channel at that particular link at the specific frequency, as well as the interference pattern it generates.

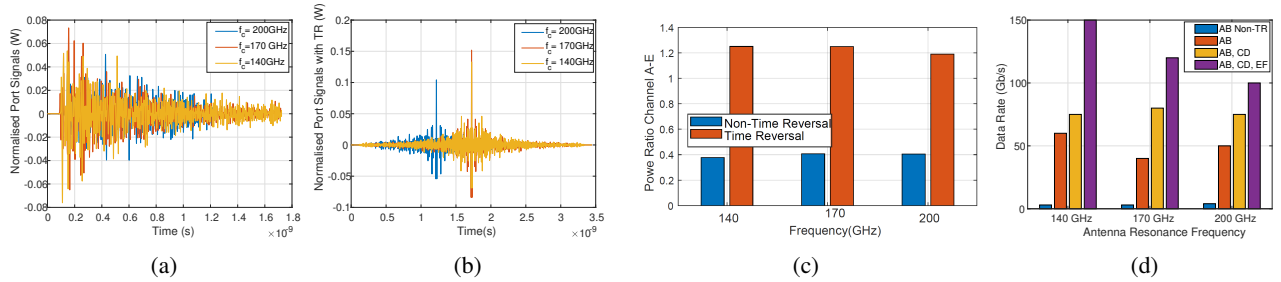


Fig. 6: Impact of the resonant frequency of the antennas on the validity of the TR approach. (a) CIR for the *AE* link without time reversal and (b) with time reversal. (c) Power concentrated on the desired target node *E* divided by the power received at the rest of the terminals. (d) Aggregated data rate with different techniques and number of concurrent links for BER of 0.1 and 0 dBm per transmitter.

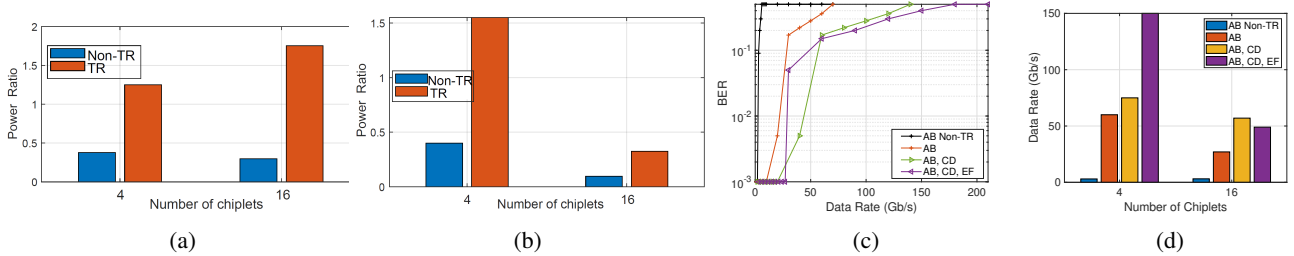


Fig. 7: Impact of the number of chiplets and their dimensions on the validity of the TR approach. (a) Power concentrated on the desired target to the power received by the rest of the terminals for links *AE* and *GC*, and (b) for links *GH* and *HF* in the four-chiplet and sixteen-chiplet case, respectively. (c) BER as a function of aggregate data rate for 0dBm per transmission for sixteen chiplets. (d) Aggregate data rates for BER = 0.1 and 0 dBm per transmission.

Interestingly, the single-link performance decreases from 140 GHz to 170 GHz and then rises again. Whereas the three-link performance decreases sharply when shifting from 140 GHz to higher frequencies.

B. Impact of Number of Chiplets

Next, we evaluate the TR technique in a 16 chiplets interposer. For this, some changes are made in the original configuration presented in Section II, while maintaining 140 GHz as the frequency of operation. The changes come mainly in the size of the chiplets, reduced in this case to fit 16 in the same system dimensions, and in the location of the antennas. We distribute one antenna per chiplet. Similar to the analysis done in Section VI-A, here we evaluate the ratio of the power in the target destination with respect to that of the rest of antennas, as well as the BER as a function of the data rate and the data rate at a specific BER.

Figure 7(a) and 7(b) show the comparison of the power ratio for 4 and 16 chiplets in two different links. For the 4 chiplet case, we take the channels *AE* and *GH* as examples. To perform a fair comparison with the 16 chiplet case, we find links that are in a close physical position to their 4-chiplet counterparts, which would be links *GC* and *FH* in this case. In Figure 3 we can see the position of the antennas for both scenarios.

Although the increase of chiplet-package interfaces in the sixteen-chiplet case significantly and complicates the propagation, the results from Figure 7(a) illustrate that TR can still improve the field concentration. However, there is a strong dependence on the relative positions of the chiplets, as we can see in Figure 7(b) for sixteen chiplets. In that case, both

the power of the non-TR and TR are reduced as propagation impairments prevent a large part of the energy to reach the chiplet of node *H* from node *F*. The difference among both shrinks.

Next, Figure 7(c) plots the BER as a function of the data rate. We observe that, as a consequence of the better spatial and temporal focusing suggested in previous figures, the achievable data rate is higher in the TR case. The sixteen-chiplet case admits two concurrent transmissions with relative ease, at least for the two links selected here. However, as we add a third link, noise and interference seems to dominate, to the point of not achieving a better performance than in the two-link case. The comparison made in Figure 7(d) for BER=0.1 further illustrates the difference between the two analyzed cases. This result indeed suggests that the more complex channel leads to the existence of higher correlations and, hence, higher interference even with TR. Also, the losses in the channel may be increasing, leading to a higher impact of the noise existing in all receivers. That would also explain the lower data rate in the single-link case.

VII. PERFORMANCE DEGRADATION WITH NON-IDEAL FILTERS

The spatial-temporal concentration of ideal TR filters has demonstrated superior performance on higher bandwidths up to 50 Gb/s thanks to the mitigation of ISI effects. However, so far we assumed that the TR filters have been implemented with perfect synchronized sampling of the pre-characterized CIR with infinite sampling speed. In practice, however, a digital filter implementing TR would need to have a finite sampling rate to be feasible.

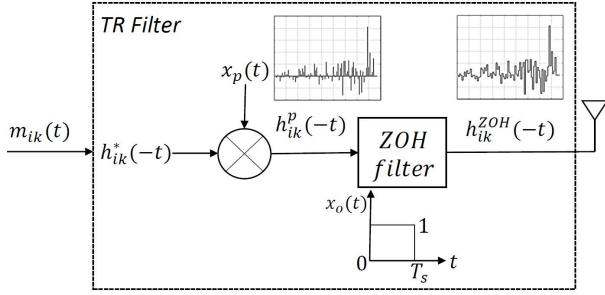


Fig. 8: Overview of zero-order hold filtering.

Ideally, the filter needs to capture all the temporal variations of the channel to perfectly apply TR on a given channel. However, our full-wave simulations have shown that due to the high frequencies involved and the densely integrated environment being simulated, changes in the response in picosecond time intervals, which would need sampling frequencies in the THz range to be captured. Implementation of filters with such resolution is unfeasible. Therefore, based on realistic constraints, it is important to analyze the impact of TR with non-ideal filters and evaluate the spatial-temporal focusing based on the trade-off between the resource constraints and the received signal strength.

A. Zero-Order Hold Filter

Inspired by the standard interpolation technique of sample and hold [45], here we propose a simple analysis considering the ideal TR estimation and hold the amplitude to the period of reduced sampling frequency. With this method, the sampled amplitudes are being held constant at the point of sampling operation is performed simply by introducing a synchronized square wave to the sampled signal with equal sampling frequency. This operation is identified as zero-order hold (ZOH) filtering. ZOH filter holds each sampled value for a duration of one sampling interval, as it is illustrated in Figure 8.

Since the nearest received multi-path components on the CIR have approximately equal amplitudes, the preserved amplitudes with ZOH filtering have a similar effect on the concentrated energy with reduced sample rates along with a minor degradation of energy concentration. We next evaluate the impact of reducing the sampling frequency.

B. Performance Evaluation

The general behavior of the ZOH filtering of the CIR is illustrated in Figure 9. As can be observed, the ideal TR response which acts as the perfect filter has a quickly oscillating behavior. The second chart shows how the ZOH filter has reduced the sampling frequency down to 100GHz, with noticeable non-linearities appearing due to the ZOH operation. Still, at 100 GHz, we still can see the high-energy components of the filter around 1.4 ns and 1.6 ns are still distinguishable. As ZOH acts as a typical low pass filter in the time domain, the frequency domain response corresponds to a $\text{sinc}(\cdot)$ function, which in return could limit the frequency

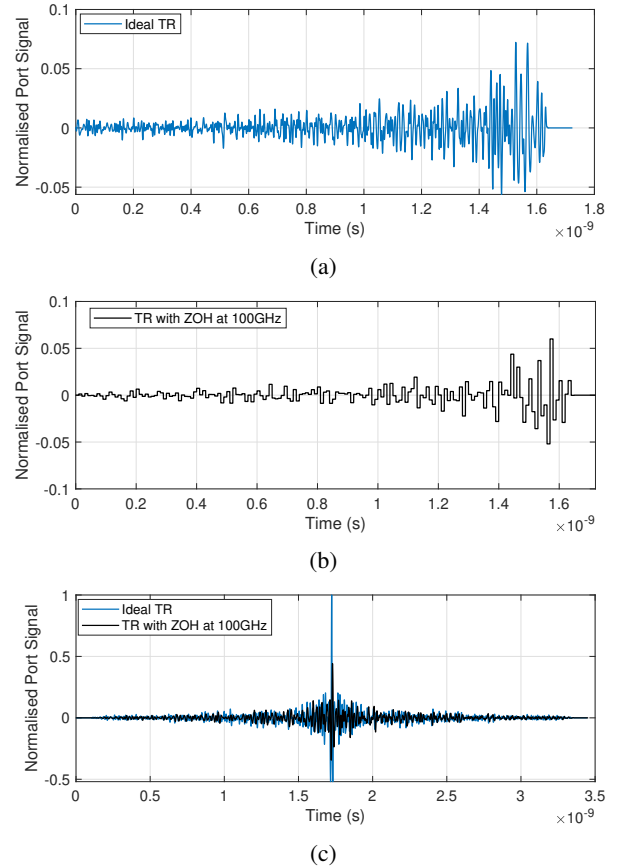


Fig. 9: Impact of the use of non-ideal filters on the response of the TR channel. (a) Response of the ideal TR filter. (b) Response of the TR filter with ZOH at 100 GHz sampling frequency. (c) Comparison of energy concentration with ideal TR filter and ZOH.

components. Hence, if the sampling frequency is reduced further, significant portions of the CIR could be lost in the filter. Finally, Figure 9(c) illustrates the difference between the convolution of the filter and the channel in both cases. We observe how the ideal TR has a higher energy in the peak and in the surroundings, whereas the ZOH version, even sampled at a very high frequency, has a slight broadening of the response.

To evaluate the performance of the technique sample and hold, we summarize the results of several evaluations in Figure 10. First, we integrate the energy around the peak with a window of 0.4 ns (corresponding to a modulation speed of 2.5 Gb/s) and compare it to the energy outside of the peak, as an indication of how well the temporal concentration is maintained when sampling at different frequencies. As shown in Figure 10(a), the energy is rather constant until the sampling rate drops below 350 GHz. As we shift further down, there is a degradation of the ratio, yet without a drop of more than 7 dB until 50GHz sampling frequency.

Furthermore, the effect of I_{SISO} was measured by varying the window size of the interference measurement. This result provides us with an approximate idea on measured signal strength when the data rate is increased (and then the window reduced). From the results of Figure 10(b), it is apparent that when the window size is increased, the amount of captured

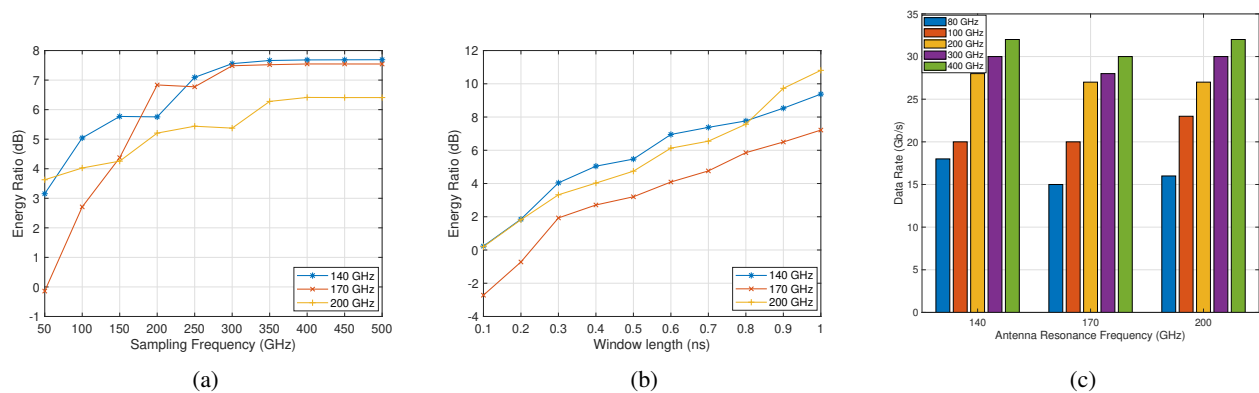


Fig. 10: Impact of the TR filter properties on the performance of TR for the 140 GHz, 170 GHz, and 200 GHz channels. (a) Ratio of energy within a window of 0.4 ns centered in the peak of the response, to that outside the window as a function of the sampling frequency. (b) Ratio of energy within a window of variable size to that outside the window as a function of the window size, for a sampling rate of 100 GHz. (c) Achievable data rate as a function of the sampling rate of the TR filter at 0.1 BER and 0 dBm.

energy also increases proportionally. In the figure we see that the impact of the window size is more noticeable at small sizes, since the finite sampling rates causes the peak to broaden. The impact of the resonance frequency is mild.

Finally, to analyze the performance of the filter with BER, the data rates were evaluated with varied sampling frequencies (i.e. 400 GHz, 300 GHz, 200 GHz, 100 GHz, and 80 GHz) for three resonance frequencies. As illustrated in Figure 10(c) for a fixed BER of 0.1, the achievable data rates seem to degrade gracefully as we reduce the sampling rate by significant amounts, still achieving remarkable speeds for a sampling rate of 80 GHz.

VIII. CONCLUSION

In this paper, we have presented the idea of applying time reversal to mitigate the sources of interference in static wireless communication scenarios within computing packages. To explore the effect of TR in varied setups, we evaluated the technique in a base scenario with four chiplets and antennas operating at 140 GHz, assuming ideal TR filters, as well as for multiple variations in frequency, geometry, and also employing TR filters with finite sampling rate. Overall, the results proved the superior capabilities of TR in transmission, obtaining a remarkable amount of power concentration in targeted destinations. The performance of TR in transmission was assessed by calculating the error rate as a function of the data rate. We observed that TR provides an order-of-magnitude improvement with respect to non-TR transmissions, and that allows to perform 2–3 concurrent transmissions to further boost the data rate. We did not observe a clear variation with frequency, because the environment under evaluation is reverberant at all the evaluated frequencies. When increasing the number of chiplets, the changes were significant due to the higher complexity of a channel with numerous changes of propagation medium. Finally, we evaluated the impact of a finite sampling frequency in the TR filter on the performance of the technique. We observed a rather graceful degradation of the achievable data rate. In future work, we aim to explore

the limits of the technique as we further reduce the sampling rate and further simplify the filter.

REFERENCES

- [1] G. Nychis, C. Fallin, T. Moscibroda, O. Mutlu, and S. Seshan, "On-chip networks from a networking perspective: congestion and scalability in many-core interconnects," in *Proceedings of the SIGCOMM*, 2012, pp. 407–18.
- [2] B. Zimmer, R. Venkatesan, Y. S. Shao, J. Clemons, M. Fojtik, N. Jiang, B. Keller, A. Klinefelter, N. Pinckney, P. Raina *et al.*, "A 0.32–128 tops, scalable multi-chip-module-based deep neural network inference accelerator with ground-referenced signaling in 16 nm," *IEEE Journal of Solid-State Circuits*, vol. 55, no. 4, pp. 920–932, 2020.
- [3] F. Lemic, S. Abadal, W. Tavernier, P. Stroobant, D. Colle, E. Alarcón, J. Marquez-Barja, and J. Famaey, "Survey on terahertz nanocommunication and networking: A top-down perspective," *IEEE Journal on Selected Areas in Communications*, vol. 39, no. 6, pp. 1506–1543, 2021.
- [4] H. Elayan, R. M. Shubair, J. M. Jornet, and P. Johari, "Terahertz channel model and link budget analysis for intrabody nanoscale communication," *IEEE transactions on nanobioscience*, vol. 16, no. 6, pp. 491–503, 2017.
- [5] A. Todri-Sanial, R. Ramos, H. Okuno, J. Dijon, A. Dhavamani, M. Wislicenus, K. Lilienthal, B. Uhlig, T. Sadi, V. Georgiev, A. Asenov, S. Amoroso, A. Pender, A. Brown, C. Millar, F. Motzfeld, B. Gotsmann, J. Liang, G. Gonçalves, N. Rupasinghe, and K. Teo, "A Survey of Carbon Nanotube Interconnects for Energy Efficient Integrated Circuits," *IEEE Circuits and Systems Magazine*, vol. 17, no. 2, pp. 47–62, 2017.
- [6] X. Timoneda, S. Abadal, A. Franques, D. Manassis, J. Zhou, J. Torrellas, E. Alarcón, and A. Cabellos-Aparicio, "Engineer the channel and adapt to it: Enabling wireless intra-chip communication," *IEEE Transactions on Communications*, vol. 68, no. 5, pp. 3247–3258, 2020.
- [7] S. Deb, A. Ganguly, P. P. Pande, B. Belzer, and D. Heo, "Wireless NoC as Interconnection Backbone for Multicore Chips: Promises and Challenges," *IEEE Journal on Emerging and Selected Topics in Circuits and Systems*, vol. 2, no. 2, pp. 228–239, 2012.
- [8] A. K. Kodi, A. I. Sikder, D. Ditomaso, S. Kaya, D. Matolak, and W. Rayess, "Kilo-core Wireless Network-on-Chips (NoCs) Architectures," in *Proceedings of the NANOCOM '15*, 2015, p. Art. 33.
- [9] S. Shamim, N. Mansoor, R. S. Narde, V. Kothandapani, A. Ganguly, and J. Venkataraman, "A Wireless Interconnection Framework for Seamless Inter and Intra-chip Communication in Multichip Systems," *IEEE Transactions on Computers*, vol. 66, no. 3, pp. 389–402, 2017.
- [10] S. Abadal, A. Mestres, J. Torrellas, E. Alarcón, and A. Cabellos-Aparicio, "Medium access control in wireless network-on-chip: A context analysis," *IEEE Communications Magazine*, vol. 56, no. 6, pp. 172–178, 2018.
- [11] V. Pano, I. Tekin, I. Yilmaz, Y. Liu, K. R. Dandekar, and B. Taskin, "TSV antennas for multi-band wireless communication," *IEEE Journal on Emerging and Selected Topics in Circuits and Systems*, vol. 10, no. 1, pp. 100–113, 2020.

- [12] A. Karkar, T. Mak, K.-F. Tong, and A. Yakovlev, "A Survey of Emerging Interconnects for On-Chip Efficient Multicast and Broadcast in Many-Cores," *IEEE Circuits and Systems Magazine*, vol. 16, no. 1, pp. 58–72, 2016.
- [13] D. Matolak, S. Kaya, and A. Kodi, "Channel modeling for wireless networks-on-chips," *IEEE Communications Magazine*, vol. 51, no. 6, pp. 180–186, 2013.
- [14] J. W. Holloway, G. C. Dogiamis, and R. Han, "A 105Gb/s Dielectric-Waveguide Link in 130nm BiCMOS Using Channelized 220-to-335GHz Signal and Integrated Waveguide Coupler," in *Proceedings of the ISSCC '21*, 2021, pp. 27–29.
- [15] C. Yi, D. Kim, S. Solanki, J. H. Kwon, M. Kim, S. Jeon, Y. C. Ko, and I. Lee, "Design and Performance Analysis of THz Wireless Communication Systems for Chip-to-Chip and Personal Area Networks Applications," *IEEE Journal on Selected Areas in Communications*, vol. 39, no. 6, pp. 1785–1796, 2021.
- [16] J. M. Jornet and I. F. Akyildiz, "Femtosecond-long pulse-based modulation for terahertz band communication in nanonetworks," *IEEE Transactions on Communications*, vol. 62, no. 5, pp. 1742–1754, 2014.
- [17] A. Franques, S. Abadal, H. Hassanieh, and J. Torrellas, "Fuzzy-token: An adaptive mac protocol for wireless-enabled manycores," in *2021 Design, Automation & Test in Europe Conference & Exhibition (DATE)*. IEEE, 2021, pp. 1657–1662.
- [18] D. Bertozzi, G. Dimitrakopoulos, J. Flich, and S. Sonntag, "The fast evolving landscape of on-chip communication," *Design Automation for Embedded Systems*, vol. 19, no. 1, pp. 59–76, 2015.
- [19] G. Lerosey, J. De Rosny, A. Tourin, A. Derode, G. Montaldo, and M. Fink, "Time reversal of electromagnetic waves," *Physical review letters*, vol. 92, no. 19, p. 193904, 2004.
- [20] G. Lerosey, J. De Rosny, A. Tourin, and M. Fink, "Focusing beyond the diffraction limit with far-field time reversal," *Science*, vol. 315, no. 5815, pp. 1120–1122, 2007.
- [21] F. Han, Y. H. Yang, B. Wang, Y. Wu, and K. J. Liu, "Time-reversal division multiple access over multi-path channels," *IEEE Transactions on Communications*, vol. 60, no. 7, pp. 1953–1965, 2012.
- [22] Q. Xu, C. Jiang, Y. Han, B. Wang, and K. J. Liu, "Waveforming: An Overview With Beamforming," *IEEE Communications Surveys and Tutorials*, vol. 20, no. 1, pp. 132–149, 2018.
- [23] G. C. Alexandropoulos, A. Mokh, R. Khayat-zadeh, J. de Rosny, M. Kamoun, A. Ourir, A. Tourin, M. Fink, and M. Debbah, "Time reversal for 6g spatiotemporal focusing: Recent experiments, opportunities, and challenges," *IEEE Vehicular Technology Magazine*, 2022.
- [24] M. J. Chabalko and A. P. Sample, "Electromagnetic time reversal focusing of near field waves in metamaterials," *Applied Physics Letters*, vol. 109, no. 26, 2016.
- [25] A. Bandara, F. Rodríguez-Galán, E. P. de Santana, P. H. Bolívar, E. Alarcón, and S. Abadal, "Exploration of time reversal for wireless communications within computing packages," *Proceedings of the 10th ACM International Conference on Nanoscale Computing and Communication (NANOCOM)*, 2023.
- [26] F. Rodríguez-Galán, A. Bandara, E. P. de Santana, P. H. Bolívar, S. Abadal, and E. Alarcón, "Collective communication patterns using time-reversal terahertz links at the chip scale," in *Proceedings of IEEE Global Communications Conference (GLOBECOM)*, 2023.
- [27] G. Bellanca, G. Calò, A. E. Kaplan, P. Bassi, and V. Petruzzelli, "Integrated vivaldi plasmonic antenna for wireless on-chip optical communications," *Optics express*, vol. 25, no. 14, pp. 16214–16227, 2017.
- [28] W. Rayess, D. W. Matolak, S. Kaya, and A. K. Kodi, "Antennas and Channel Characteristics for Wireless Networks on Chips," *Wireless Personal Communications*, vol. 95, no. 4, pp. 5039–5056, 2017.
- [29] X. Timoneda, A. Cabellos-Aparicio, D. Manassis, E. Alarcón, and S. Abadal, "Channel characterization for chip-scale wireless communications within computing packages," in *2018 Twelfth IEEE/ACM International Symposium on Networks-on-Chip (NOCS)*. IEEE, 2018, pp. 1–8.
- [30] F. Gutierrez, S. Agarwal, K. Parrish, and T. S. Rappaport, "On-chip integrated antenna structures in cmos for 60 ghz wpan systems," *IEEE Journal on Selected Areas in Communications*, vol. 27, no. 8, pp. 1367–1378, 2009.
- [31] H.-H. Yeh, N. Hiramatsu, and K. L. Melde, "The design of broadband 60 ghz amc antenna in multi-chip rf data transmission," *IEEE Transactions on Antennas and Propagation*, vol. 61, no. 4, pp. 1623–1630, 2012.
- [32] S. Hwangbo, R. Bowrothu, H.-i. Kim, and Y.-K. Yoon, "Integrated compact planar inverted-f antenna (pifa) with a shorting via wall for millimeter-wave wireless chip-to-chip (c2c) communications in 3d-sip," in *2019 IEEE 69th Electronic Components and Technology Conference (ECTC)*. IEEE, 2019, pp. 983–988.
- [33] K. Duraisamy, R. G. Kim, and P. P. Pande, "Enhancing performance of wireless noocs with distributed mac protocols," in *Sixteenth International Symposium on Quality Electronic Design*. IEEE, 2015, pp. 406–411.
- [34] N. Mansoor and A. Ganguly, "Reconfigurable wireless network-on-chip with a dynamic medium access mechanism," in *Proceedings of the 9th International Symposium on Networks-on-Chip*, 2015, pp. 1–8.
- [35] B. Ollé, P. Talarn, A. Cabellos-Aparicio, F. Lemic, E. Alarcón, and S. Abadal, "Multi-channel medium access control protocols for wireless networks within computing packages," in *2023 IEEE International Symposium on Circuits and Systems (ISCAS)*, 2023, pp. 1–5.
- [36] A. Ganguly, S. Abadal, I. Thakkar, N. E. Jerger, M. Riedel, M. Babaie, R. Balasubramonian, A. Sebastian, S. Pasricha, and B. Taskin, "Interconnects for dna, quantum, in-memory, and optical computing: Insights from a panel discussion," *IEEE micro*, vol. 42, no. 3, pp. 40–49, 2022.
- [37] S. Abadal, C. Han, and J. M. Jornet, "Wave propagation and channel modeling in chip-scale wireless communications: A survey from millimeter-wave to terahertz and optics," *IEEE access*, vol. 8, pp. 278–293, 2019.
- [38] Y. Chen and C. Han, "Channel modeling and characterization for wireless networks-on-chip communications in the millimeter wave and terahertz bands," *IEEE Transactions on Molecular, Biological and Multi-Scale Communications*, vol. 5, no. 1, pp. 30–43, 2019.
- [39] O. Markish, O. Katz, B. Sheinman, D. Corcos, and D. Elad, "On-chip millimeter wave antennas and transceivers," in *Proceedings of the 9th International Symposium on Networks-on-Chip*, 2015, pp. 1–7.
- [40] S. Wright, R. Polastre, H. Gan, L. Buchwalter, R. Horton, P. Andry, E. Sprogis, C. Patel, C. Tsang, J. Knickerbocker *et al.*, "Characterization of micro-bump c4 interconnects for si-carrier sop applications," in *56th Electronic Components and Technology Conference 2006*. IEEE, 2006, pp. 8–pp.
- [41] X. Zhang, J. K. Lin, S. Wickramanayaka, S. Zhang, R. Weerasekera, R. Dutta, K. F. Chang, K.-J. Chui, H. Y. Li, D. S. Wee Ho *et al.*, "Heterogeneous 2.5 d integration on through silicon interposer," *Applied physics reviews*, vol. 2, no. 2, 2015.
- [42] A. Kannan, N. E. Jerger, and G. H. Loh, "Enabling interposer-based disintegration of multi-core processors," in *Proceedings of the 48th international symposium on Microarchitecture*, 2015, pp. 546–558.
- [43] M. F. Imani, S. Abadal, and P. del Hougne, "Metasurface-programmable wireless network-on-chip," *Advanced Science*, 2022.
- [44] Computer Simulation Technology (CST), "CST Microwave Studio," 2022. [Online]. Available: <http://www.cst.com>
- [45] A. Oppenheim, A. Willsky, and I. Young, *Signals and Systems*. Prentice-Hall, Englewood Cliffs, New Jersey, 1983.